

## Thermodynamics of 2+1 flavour QCD

---

**Jan van der Heide\***, RBC-Bielefeld collaboration

*Fakultät für Physik, Universität Bielefeld, D33615, Bielefeld, Germany*

*E-mail: [jan@physik.uni-bielefeld.de](mailto:jan@physik.uni-bielefeld.de)*

Recent results on QCD thermodynamics from the RBC-Bielefeld collaboration will be presented. The simulations have been performed on  $16^3 \times 4$ ,  $24^3 \times 6$  and the corresponding zero temperature lattices. The quark masses are tuned such that the light pseudoscalar meson has a mass of about 200 MeV and the Kaon adopts its physical mass.

*The XXV International Symposium on Lattice Field Theory  
July 30 - August 4 2007  
Regensburg, Germany*

---

\*Speaker.

## 1. Introduction

Obtaining detailed knowledge of the temperature dependence of the pressure and energy density, *i.e.* the equation of state, is very important for the understanding the behaviour of the fireball created in heavy ion collisions. Several results for the equation of state in the two limiting cases have been obtained. While the low temperature regime might be adequately described by the hadron resonance gas model [1], and at very high temperatures, perturbation theory ought to work [2], both techniques fail to correctly describe the transition from the hadronic regime to the plasma phase; here one has to resort to genuinely non-perturbative methods such as lattice QCD. In this paper, we present results for the QCD equation of state with almost physical quark masses. We performed our calculations with a Symanzik improved gauge action and the p4fat3 fermion action to reduce cut-off effects. In Sec.2, we introduce the necessary thermodynamic background, Sec.?? deals with the line of constant physics, the simulation parameters are discussed in Sec.3, whereafter the results are presented in Sec.4. We end with conclusions in Sec.5.

## 2. Equation of State

The grand canonical potential is defined as

$$\Omega(T, V) = T \ln Z(T, V) - \Omega_0 \quad (2.1)$$

where we use the normalisation  $\Omega_0 = \lim_{T \rightarrow 0} T \ln Z(T, V)$  to remove ultraviolet divergences. The pressure and energy density are then simply obtained by invoking standard thermodynamic relations:

$$p = \frac{1}{V} \Omega(T, V), \quad \varepsilon = \frac{T^2}{V} \frac{\partial \Omega(T, V) / T}{\partial T} \quad (2.2)$$

Due to our normalisation,  $p$  and  $\varepsilon$  both vanish at  $T = 0$  by construction. This choice is similar to that used in *e.g.* hadron gas calculations [1], but differs from normalisations used in other methods [3, 4]. This should be kept in mind when our results are compared to other work. In the entropy density,  $s/T^3 = (p - \varepsilon)/T^4$ , this ambiguity drops out; it is thus the preferred observable for comparisons.

Since neither the grand canonical potential nor the partition function itself are directly obtainable from lattice calculations, we use the integration method[5]. We thus calculate the energy-momentum tensor

$$\frac{\theta^{\mu\mu}(T)}{T^4} \equiv \frac{\varepsilon - 3p}{T^4} = T \frac{\partial}{\partial T} (p/T^4) \quad (2.3)$$

and obtain the pressure as the temperature integral

$$\frac{p(T)}{T^4} - \frac{p(T_0)}{T_0^4} = \int_{T_0}^T dT' \frac{\theta^{\mu\mu}}{T'^5}. \quad (2.4)$$

The temperature  $T_0$  is chosen deep enough in the hadronic phase, where the pressure is already very small and can thus safely be ignored.

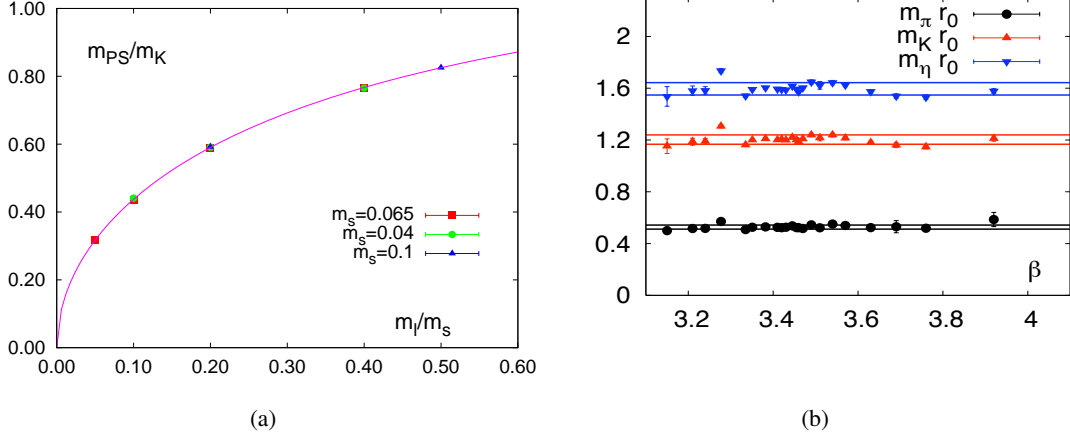


**Figure 1:** Line of constant physics: a) the ratio of  $m_{ps}/m_K$  does not depend on  $h = m_s/m_l$ . b) Meson masses along the LCP; lines denote a band of  $\pm 3\%$ .

The energy-momentum tensor can be expressed in observables which are easily calculated on the lattice,

$$\begin{aligned}
\frac{\theta^{\mu\mu}(T)}{T^4} &= -\left(\frac{N_\tau}{N_\sigma}\right)^3 \left(a \frac{d\beta}{da}\right) \frac{\partial}{\partial\beta} \ln Z \\
&= -R_\beta N_\tau^4 \left( \frac{1}{N_\sigma^3 N_\tau} \left\langle \frac{dS}{d\beta} \right\rangle_\tau - \frac{1}{N_\tau N_0} \left\langle \frac{dS}{d\beta} \right\rangle_0 \right) \\
&= R_\beta \{ [\langle S_G \rangle_0 - \langle S_G \rangle_\tau] - R_m [2\hat{m}_l (\langle \bar{\psi}\psi \rangle_{l,0} - \langle \bar{\psi}\psi \rangle_{l,\tau}) + \hat{m}_s (\langle \bar{\psi}\psi \rangle_{s,0} - \langle \bar{\psi}\psi \rangle_{s,\tau})] \\
&\quad - R_h \hat{m}_s (\langle \bar{\psi}\psi \rangle_{s,0} - \langle \bar{\psi}\psi \rangle_{s,\tau}) \} N_\tau^4
\end{aligned}$$

where  $\langle S_G \rangle_{0,\tau} = -\frac{1}{V} \frac{\partial}{\partial\beta} \ln Z = \frac{1}{N_\sigma^3 N_{0,\tau}} \langle S_G \rangle$  is the expectation value of the gluon action density,  $\langle \bar{\psi}\psi \rangle_q = \frac{T}{V} \frac{\partial}{\partial\hat{m}_q} \ln Z = \frac{1}{4} \frac{1}{N_\sigma^3 N_{0,\tau}} \langle \text{Tr} M^{-1}(\hat{m}_q) \rangle$  is the chiral condensate for quark flavour  $q$ , and  $\hat{m}_q = m_q a$  is the dimensionless quark mass. Furthermore, since we have changed the temperature derivative to a derivative with respect to  $\beta$ , one needs the 'Beta functions',

$$R_\beta = -a \frac{d\beta}{da} = \frac{r_0}{a} \left( \frac{dr_0/a}{d\beta} \right)^{-1} \quad R_m = \frac{1}{\hat{m}_l} \left( \frac{\partial \hat{m}_l}{\partial \beta} \right)_h \quad R_h = \frac{1}{h} \left( \frac{\partial h}{\partial \beta} \right)_{\hat{m}_l}. \quad (2.5)$$

Where  $h = m_s/m_l$ . Using  $h$  instead of  $m_s$  enables us to remove the corresponding  $\beta$ -function altogether, as we shall see in the following section.

### 3. Simulation parameters

In this section we shortly present the main parameters we have used in our simulations. We have used lattice sizes of  $16^3 \times 4$  and  $24^3 \times 6$ . In order to reduce discretisation effects, we employ improved actions; the tree level improved  $1 \times 2$  gauge action and the p4fat3 fermion action. The use

of the p4[6] fat3 fermion action also improves the rotational and the flavour symmetry. We simulate two light and one heavier strange quark. The partition function depends on several parameters. In order to keep physics the same along the integration trajectory, we need to fine tune the bare parameters.

$$Z(T, V; g, m_l, m_s) = Z(N_\tau, N_\sigma, a; \beta, \hat{m}_l, \hat{m}_s) \rightarrow Z(N_\tau, N_\sigma, a; \beta, m_\pi, m_K) \quad (3.1)$$

For different  $\beta$ -values, we tune the bare quark masses  $\hat{m}$  such that the pion and kaon masses remain the same. From Fig.1(a), we see that to a high accuracy, the ratio of the kaon and pion masses depends only on the light quark mass and the ratio  $h = m_s/m_l$ , not on the strange quark mass separately. We choose our LCP by taking  $h = 10$ , and tuning the light quark mass such that the kaon acquires its physical mass,  $m_K = 500$  MeV, which corresponds to  $m_\pi \approx 220$ . In Fig.1(b) we show the resulting meson masses in units of a physical scale ( $r_0$ ). From this, we see that our simulations are indeed done along a line of constant physics. The line of constant physics is defined through the following constraints,  $m_{ss}r_0 = 1.58$  and  $m_\pi/m_K = 0.437$ , with  $r_0$  the Sommer scale.

To generate the Markov chain, we use the Rational Hybrid Monte Carlo (RHMC)[7, 8] as the updating method. This algorithm has the advantage that it is made exact through the Metropolis accept/reject step, allowing the use of different orders for the rational approximation in different parts of the updating scheme. For the calculation of the pseudofermion force, which is computationally the most expensive part, we choose a low order. The error made in this step is corrected for by the Metropolis step, with a high order rational polynomial. The error of this last approximation is chosen to be at the level of machine precision, which leads to an order of 20 or 16, depending on the quark mass. The order used in the force calculation is tuned such that the acceptance is about 70% at a trajectory length of 0.5. This gives an order of 16 or 10, again depending on  $m_l$ . As is normal for RHMC, we use a multishift inversion solver[9]. In order to reduce the computational costs even further, we use different time steps for the gauge and fermion parts of the updating algorithm, á la Sexton and Weingarten[10], in a ratio of 15 : 1. For every  $T, m_l$  combination, we have obtained  $\mathcal{O}(10^4)$  configurations.

## 4. Results

### 4.1 $\beta$ -functions

In order to evaluate the beta functions of Eq.2.5, we need to know the  $\beta$ -dependence of  $r_0/a(\beta)$  and  $\hat{m}_l(\beta)$ . As a parametrisation, we use a Renormalisation Group inspired rational fit ansatz,

$$\begin{aligned} \frac{r_0}{a}(\beta) &= \frac{1}{a_r R_2(\beta)} \frac{1 + e_r \hat{a}^2(\beta) + f_r \hat{a}^4(\beta)}{1 + b_r \hat{a}^2(\beta) + c_r \hat{a}^4(\beta) + d_r \hat{a}^6(\beta)} \\ \hat{m}_l(\beta) &= a_m R_2(\beta) \left( \frac{12b_0}{\beta} \right)^{4/9} \frac{1 + b_m \hat{a}^2(\beta) + c_m \hat{a}^4(\beta) + d_m \hat{a}^6(\beta)}{1 + e_m \hat{a}^2(\beta) + f_m \hat{a}^4(\beta)} \end{aligned}$$

with  $R_2(\beta)$  the perturbative  $\beta$ -function to two loops,  $R_2(\beta) = \exp\left(-\frac{\beta}{12b_0}\right) \left(\frac{6b_0}{\beta}\right)^{-b_1/(2b_0^2)}$ , and  $\hat{a}(\beta) = R_2(\beta)/R_2(\beta = 3.4)$ . In the case of  $r_0/a$ , we also used two- and three interval cubic spline fits in order to investigate the influence of the fits on the resulting  $\beta$ -function.

In Fig.2, we show the data for  $r_0/a$  and  $m_l a$  and the mentioned fits. As we can see, the rational fits seem to describe the data very well. For  $r_0/a$ , the different spline fits describe the data equally

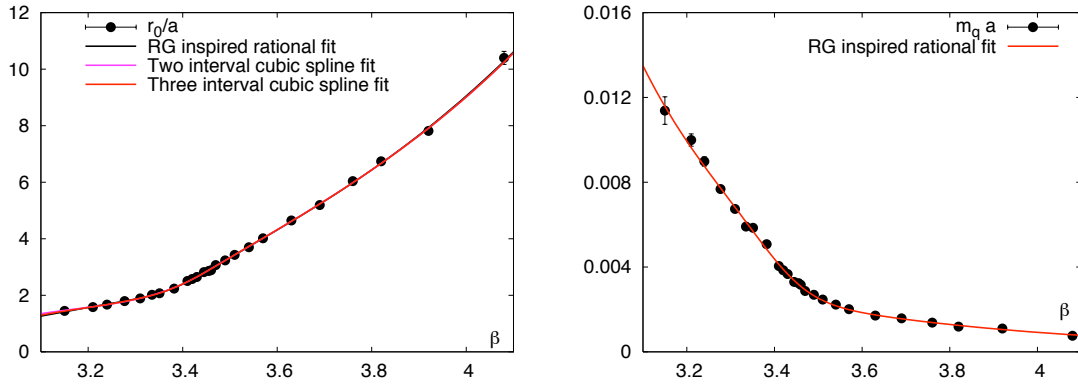


**Figure 2:** Parametrisation of  $r_0/a$  (left) and  $m_q a$  (right) in order to extract the  $\beta$ -functions

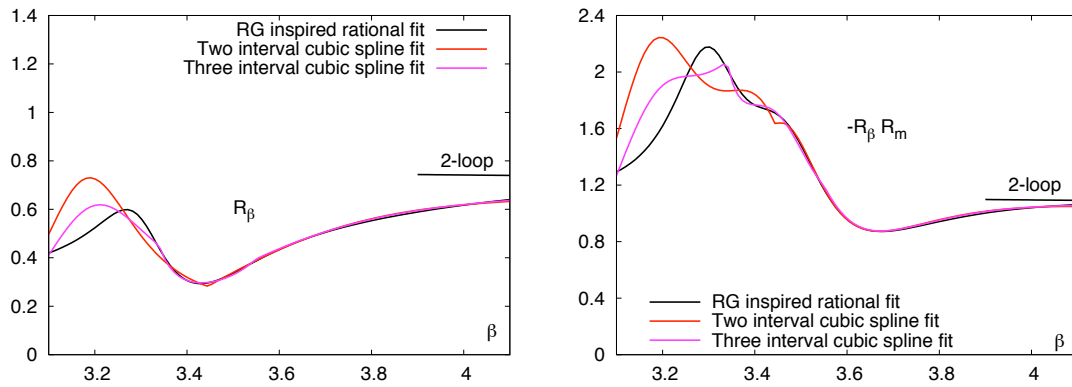


**Figure 3:**  $\beta$ -functions as obtained from the fit functions,  $R_\beta$  (left) and  $-R_\beta R_m$  (right).

well. The resulting  $\beta$ -functions extracted from these fits are shown in Fig.3. Although the different fits are very similar, the resulting  $\beta$ -functions show somewhat different behaviour at low  $\beta$  values. The differences are not large and will only have a small influence on the thermodynamic variables. Moreover, the differences only occur for  $\beta$  values that are used in the  $n_\tau = 4$  simulations. The low  $\beta$  domain is still under investigation, therefore, the results we show in the next section are obtained using the RG inspired fit only, without implying its superiority.

## 4.2 Equation of state

In this section, we present the main results of our investigation. For details and a more thorough discussion, confer [11]. In Fig.4 we show the trace of the energy momentum tensor,  $\theta^{\mu\mu}$ , for both values of  $N_\tau$ . As can be seen, the results are similar, but the curves do not lie on top of each other. This implies that cut-off effects are present, but small. Specifically, at low temperatures, the  $N_\tau = 4$  results are somewhat smaller. This is expected and consistent with an overall shift of the temperature scale due to the cut-off dependence of the transition temperature [12]. The peak for  $N_\tau = 4$  is somewhat higher, which is probably due to the non-perturbative structure of the  $\beta$ -functions,  $R_\beta$  and  $R_\beta R_m$  in this region. At high temperatures, the cut-off effects again become visible. The  $N_\tau = 6$  curve decreases slower with temperature than the  $N_\tau = 4$  curve. This is not a finite volume effect as we have checked with additional simulation at larger lattices. Since the contribution of the chiral condensates to  $\Theta^{\mu\mu}$  is small ( $\mathcal{O}(10\%)$ ), the observed differences can thus be attributed to cut-off effects in the gluonic sector. First calculations performed on  $N_\tau = 8$  lattices in this high temperature region are consistent with the results obtained on  $N_\tau = 6$  lattices and thus suggest that the cut-off effects are small on lattices with temporal extent  $N_\tau \geq 6$ .

From the energy momentum tensor we calculate the pressure (difference) by integration, see Eq.2.4. We used the trapezoid rule and have set the pressure to zero at our lowest  $\beta$ -value. We obtain the results displayed in Fig.5. Other integration methods produce the same results within a few percent. In Fig.5, we also show the energy density, which we obtain by combining the pressure and the energy momentum tensor. Again, the cut-off effects are seen to be small. Both curves approach the Stefan-Boltzmann limit to within 10% at high temperatures. Finally, we combine the energy density and pressure to obtain the entropy density, which is shown in Fig.5. As mentioned earlier, for this observable, the normalisation ambiguity at  $T = 0$  does not exist, and it is therefore well suited for comparison with different methods. For high temperatures, also the entropy density reaches the SB limit to within 10%.

## 5. Conclusions

We have presented the results of an extensive investigation of the equation of state in QCD with almost physical quark masses. We have performed simulations with a physical strange quark mass and two degenerate light quark masses which are only twice the physical value. Furthermore, we used larger spatial lattices than before for two different temporal extensions. The finite temperature simulations are accompanied by extensive  $T = 0$  calculations to provide the necessary normalisations and  $\beta$ -functions.

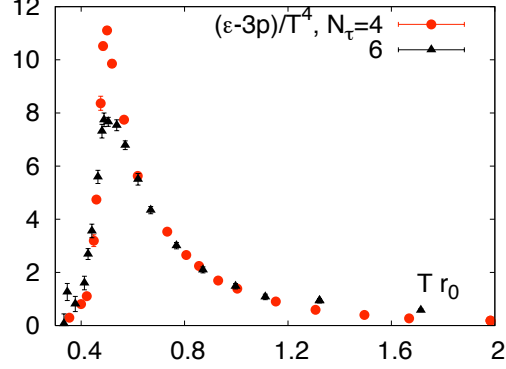


**Figure 4:** The trace of the energy momentum tensor for two values of the temporal extent,  $N_\tau$

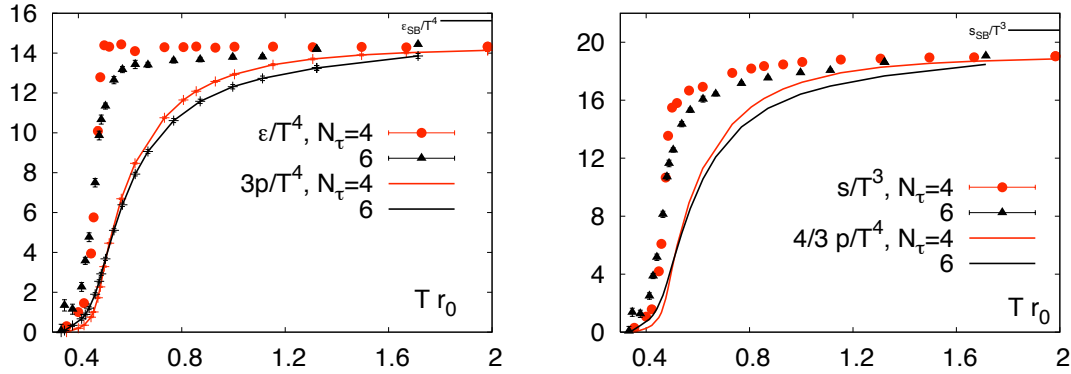


**Figure 5:** The pressure and energy density (left) and entropy density (right) as a function of temperature.

At high temperatures, bulk thermodynamic quantities as pressure, energy density, and entropy density, deviate from the continuum Stefan-Boltzmann limit only by about 10% and show little cut-off dependence. Cut-off effects are small but visible in the energy momentum tensor. These systematic effects will be resolved through further calculations on finer lattices.

## References

- [1] P. Braun-Munzinger, K. Redlich, and J. Stachel [nucl-th/0304013](#). Published in \*Quark gluon plasma III, Hwa, R.C. (ed.) et al.\*.
- [2] K. Kajantie, M. Laine, K. Rummukainen, and Y. Schroder *Phys. Rev.* **D67** (2003) 105008, [[hep-ph/0211321](#)].
- [3] A. Vuorinen *Phys. Rev.* **D68** (2003) 054017, [[hep-ph/0305183](#)].
- [4] M. Bluhm, B. Kampfer, R. Schulze, D. Seipt, and U. Heinz [arXiv:0705.0397](#) [[hep-ph](#)].
- [5] J. Engels, F. Karsch, H. Satz, and I. Montvay *Phys. Lett.* **B101** (1981) 89.
- [6] U. M. Heller, F. Karsch, and B. Sturm *Phys. Rev.* **D60** (1999) 114502, [[hep-lat/9901010](#)].
- [7] A. D. Kennedy, I. Horvath, and S. Sint *Nucl. Phys. Proc. Suppl.* **73** (1999) 834–836, [[hep-lat/9809092](#)].
- [8] M. A. Clark, A. D. Kennedy, and Z. Sroczynski *Nucl. Phys. Proc. Suppl.* **140** (2005) 835–837, [[hep-lat/0409133](#)].
- [9] B. Jegerlehner [hep-lat/9612014](#).
- [10] D. H. Weingarten and J. C. Sexton *Nucl. Phys. Proc. Suppl.* **26** (1992) 613–616.
- [11] M. Cheng et al. [arXiv:0710.0354](#) [[hep-lat](#)].
- [12] M. Cheng et al. *Phys. Rev.* **D74** (2006) 054507, [[hep-lat/0608013](#)].